Performance Analysis of Multi-frequency GNSS Carrier Tracking for Strong Ionospheric Scintillation Mitigation

Jordi Vilà-Valls
Centre Tecnològic de Telecomunicacions de Catalunya (CTTC/CERCA)
08860, Barcelona, Spain
E-mail: jvila@cttc.cat

Pau Closas
Dept. of Electrical and Computer Eng.
Northeastern University
Boston, MA 02115, USA
Email: closas@northeastern.edu

James T. Curran
European Space Agency (ESA)
Noordwijk, The Netherlands
E-mail: jamestcurran@ieee.org

***Abstract*—In Global Navigation Satellite Systems (GNSS), ionospheric scintillation is one of the more challenging propagation scenarios, particularly affecting high-precision receivers based on carrier phase measurements. In this contribution, we propose a new digital carrier synchronization state-space formulation for the mitigation of strong scintillation. It takes into account multi-frequency GNSS observations, allowing tracking of both line-of-sight phase variations and complex gain scintillation components, that is, scintillation amplitude and phase. The joint carrier tracking and scintillation mitigation problem is solved using a multi-frequency nonlinear Kalman filter-based solution. The performance improvement of the new approach is shown using realistic synthetic data, and compared to state-of-the-art PLL and KF-based architectures.**

I. Introduction

Global Navigation Satellite Systems (GNSS) is the technology of choice for most position-related applications. A GNSS receiver relies on a constellation of satellites (e.g. GPS, Galileo, or GLONASS) to estimate a set of range measures from which to compute its position. The main challenges of GNSS technology involve operation in complex, harsh propagation scenarios which are naturally impaired by multipath, shadowing, high dynamics, or ionospheric scintillation. In the last decade the mitigation of such vulnerabilities has been the main driver on advanced receiver design with the ultimate goal of providing position accuracy and reliability [1].

Among those challenges, ionospheric scintillation mitigation is certainly one of the more challenging and appealing scenarios for signal processing practitioners. Because such disturbance is not related to the local environment, as in the case of multipath or shadowing, it can degrade receiver performance even under ideal open-sky conditions. Ionospheric scintillation is caused by a disturbance in the portion of the ionosphere through which the GNSS signals propagates [2]. It can produce rapidly varying constructive and destructive interference between multiple scattered signals. This turbulent behavior can render the carrier phase difficult to track by the receiver. One of the major challenges of severe scintillation propagation conditions is the so-called canonical fades, which results in a combination of strong fading and rapid phase changes in a simultaneous and random manner [2], [3]. From a synchronization standpoint, counteracting such effect is very challenging, because the receiver has to track the faster phase changes using the worst signal level. This may lead the receiver to momentarily lose carrier synchronization, resulting in either cycle-slips or loss of lock.

Interestingly, owing to the differing wavelengths, constructive and destructive interference experienced on different frequencies can be incoherent, with the effect that deep fades tend to occur at different times on different frequencies. This paper leverages on this idea and proposes a carrier tracking method that jointly processes signals at multiple GNSS frequencies. The paper extends our previous work on single-frequency carrier tracking loops under scintillation conditions [4], [5], for which a state-space formulation and a Kalman filter (KF) were analyzed. Here, an augmented state-space formulation considering multiple frequencies is exploited and a tracking method proposed. The resulting method is validated with the Cornell Scintillation Model (CSM) [3], a popular synthetic signal simulator that generates scintillation amplitude and phase traces.

Notice that even if the trend of next-generation receivers is to consider multi-constellation observations rather than multi-frequency solutions, this is particularly useful for standard accuracy positioning (where ionospheric errors are less dominant) or when a real-time-kinematic (RTK) network is available. But there are many applications where high-accuracy is required and ionospheric impairments should be removed, motivating the interest multi-frequency architectures [6].

II. Multi-frequency GNSS and Ionospheric Scintillation Signal Model

A. Ionospheric Scintillation Signal Model

In general, scintillation can be modeled as a multiplicative channel affecting radio waves coming from space through the ionosphere. GNSS signals are typically affected by fast amplitude and phase variations [2], which may compromise the synchronization step of the receiver. Considering $s(t)$ to be

ISBN 978-0-9928626-7-1

the baseband equivalent of the transmitted signal, the received baseband signal, $x(t)$, can be expressed as,

$$x(t) = \xi_s(t)s(t) + w(t),\ \xi_s(t) = \rho_s(t)e^{j\theta_s(t)}, \quad (1)$$

where $\rho_s(t)$ and $\theta_s(t)$ are the ionospheric scintillation envelope and phase components, and $w(t)$ is a noise term including both thermal noise and any other disturbance. In this article we consider the strong scintillation propagation scenario, which is the most challenging in terms of carrier tracking performance. The CSM[1] is a very useful simulation tool to generate realistic scintillation synthetic data and test new carrier tracking methodologies. Two parameters, $0 < S_4 \leq 1$ and $0.1 \leq \tau_0 < 2$ s, determine the intensity and correlation of the scintillation, respectively. In general, higher S_4 and lower τ_0 lead to more severe scintillation. The scintillation amplitude strength is characterized by the index S_4, which in the strong scintillation case of interest is typically $S_4 > 0.6$ [3].

A key point in designing filters that provide robustness is to avoid the estimation/mitigation trade-off [4]. This implies that we must model the scintillation physical phenomena and embed both scintillation components into the state-space formulation. Such an approach allows us to distinguish between both phase contributions and estimate the scintillation process. It was shown in [4], [5] that these components can be fairly well approximated using an AR process as

$$\rho_{s,k} = \sum_{i=1}^{q} \gamma_i \rho_{s,k-i} + \kappa + \eta_{\rho,k},\ \ \eta_{\rho,k} \sim \mathcal{N}(0, \sigma^2_{\eta_\rho}), \quad (2)$$

$$\theta_{s,k} = \sum_{i=1}^{p} \beta_i \theta_{s,k-i} + \eta_{\theta,k},\ \ \eta_{\theta,k} \sim \mathcal{N}(0, \sigma^2_{\eta_\theta}), \quad (3)$$

with κ a constant value to allow a nonzero mean time-series, and the mean of the process equal to $\mu = \kappa/(1 - \sum_{i=1}^{q} \gamma_i)$; $\{\gamma_i, \beta_i\}$ are the set of AR coefficients, and $\{\sigma^2_{\eta_\rho}, \sigma^2_{\eta_\theta}\}$ the driving noise variances. The main problems arise in the AR model order selection, $\{q, p\}$ in (2) and (3), and the time-series analysis to obtain the AR parameters. In [4], [5], the selection using synthetic data was done somehow heuristically, only via visual inspection of the power spectral densities, which lacks of mathematical rigor. In this contribution, we provide an analysis for the model order selection based on partial autocorrelation functions (PAF), which is a basic tool commonly used in time-series analysis for model order selection [7]. Fig. 1 shows the sample PAFs, for both phase and amplitude, using CSM synthetic strong scintillation data sampled at $T_s = 10$ ms (i.e., number of representative taps in the PAF is directly related to the AR model order). It is clear that while the scintillation phase is correctly approximated by an AR(1), for the amplitude a higher order AR(3) is needed. Notice that for model order selection we can also consider, for instance, the Minimum Description Length criteria [8]. In this paper we only focus on strong scintillation mitigation (i.e., fixed model order), but an adaptive model order selection [8] could also be considered together with the proposed approach.

[1]The CSM has been embedded in the so-called Cornell Scintillation Simulation Matlab toolkit, which is available at `http://gps.ece.cornell.edu/tools.php`.

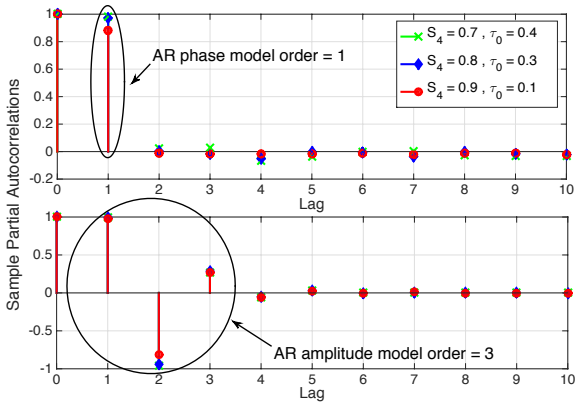

Fig. 1. PAF for both scintillation phase (top) and amplitude (bottom) for realistic CSM strong scintillation synthetic data.

B. Multi-frequency GNSS State-Space Model

Taking into account the carrier phase tracking problem at hand we make the assumption that timing is perfectly synchronized. Then after the acquisition stage, the samples at the output of the correlators can be modeled as [5]

$$y_k = \alpha_k e^{j\theta_k} + n_k,\ \ n_k \sim \mathcal{N}(0, \sigma^2_{n,k}) \quad (4)$$

where α_k and θ_k may include any non-nominal harsh propagation disturbance. Accounting for the ionospheric scintillation in the signal model leads to $\alpha_k = A_k \rho_{s,k}$ and $\theta_k = \theta_{d,k} + \theta_{s,k}$, with A_k the scintillation-free signal amplitude at the output of the correlators. The dynamics phase term $\theta_{d,k}$ refers to the line-of-sight (LOS) phase evolution due to the relative movement between satellite and receiver, and is typically modeled using a 3rd order Taylor approximation,

$$\theta_{d,k} \approx \theta_0 + 2\pi(f_{d,k} k T_s + f_{r,k} k^2 T_s^2/2), \quad (5)$$

where θ_0 (rad) is a random phase value, $f_{d,k}$ (Hz) the carrier Doppler frequency and $f_{r,k}$ (Hz/s) the Doppler rate.

In a multi-frequency architecture, a single satellite transmits simultaneously at different frequencies, therefore at the receiver side several measurements are available. Although the methodology in this paper is general for any GNSS signal, in the sequel we focus on a modern GPS triple band receiver (i.e., L_1, L_2 and L_5 bands) satellite. Then, measurements are

$$\underbrace{\begin{bmatrix} y_k^{L_1} \\ y_k^{L_2} \\ y_k^{L_5} \end{bmatrix}}_{\mathbf{y}_k} = \underbrace{\begin{bmatrix} \alpha_k^{L_1} e^{j(\theta_{d,k}^{L_1} + \theta_{s,k}^{L_1})} \\ \alpha_k^{L_2} e^{j(\theta_{d,k}^{L_2} + \theta_{s,k}^{L_2})} \\ \alpha_k^{L_5} e^{j(\theta_{d,k}^{L_5} + \theta_{s,k}^{L_5})} \end{bmatrix}}_{\mathbf{h}(\mathbf{x}_k)} + \underbrace{\begin{bmatrix} n_k^{L_1} \\ n_k^{L_2} \\ n_k^{L_5} \end{bmatrix}}_{\mathbf{n}_k}, \quad (6)$$

which may be useful to rewrite in real form as

$$\underbrace{\begin{bmatrix} y_{i,k}^{L_1} \\ y_{q,k}^{L_1} \\ y_{i,k}^{L_2} \\ y_{q,k}^{L_2} \\ y_{i,k}^{L_5} \\ y_{q,k}^{L_5} \end{bmatrix}}_{\mathbf{y}_k} = \underbrace{\begin{bmatrix} \alpha_k^{L_1} \begin{bmatrix} \cos(\theta_k^{L_1}) \\ \sin(\theta_k^{L_1}) \end{bmatrix} \\ \alpha_k^{L_2} \begin{bmatrix} \cos(\theta_k^{L_2}) \\ \sin(\theta_k^{L_2}) \end{bmatrix} \\ \alpha_k^{L_5} \begin{bmatrix} \cos(\theta_k^{L_5}) \\ \sin(\theta_k^{L_5}) \end{bmatrix} \end{bmatrix}}_{\mathbf{h}(\mathbf{x}_k)} + \underbrace{\begin{bmatrix} n_{i,k}^{L_1} \\ n_{q,k}^{L_1} \\ n_{i,k}^{L_2} \\ n_{q,k}^{L_2} \\ n_{i,k}^{L_5} \\ n_{q,k}^{L_5} \end{bmatrix}}_{\mathbf{n}_k}, \quad (7)$$

where for each frequency, $y_k = y_{i,k} + iy_{q,k}$, $\theta_k = \theta_{d,k} + \theta_{s,k}$ and $n_k = n_{i,k} + jn_{q,k}$. The different LOS carrier phase evolutions, when referencing all of the dynamics to L_1, are given by

$$\begin{bmatrix} \theta_{d,k}^{L_1} \\ \theta_{d,k}^{L_2} \\ \theta_{d,k}^{L_5} \end{bmatrix} \approx \begin{bmatrix} \theta_0^{L_1} + 2\pi(f_{d,k}kT_s + f_{r,k}k^2T_s^2/2) \\ \theta_0^{L_2} + 2\pi f_{L_2}/f_{L_1}(f_{d,k}kT_s + f_{r,k}k^2T_s^2/2) \\ \theta_0^{L_5} + 2\pi f_{L_5}/f_{L_1}(f_{d,k}kT_s + f_{r,k}k^2T_s^2/2) \end{bmatrix} \quad (8)$$

with f_{L_1}, f_{L_2} and f_{L_5} being the carrier frequencies at the different bands. Notice that the same Doppler frequency terms, $f_{d,k}$ and $f_{r,k}$, appear in all frequency bands. $\mathbf{x}_k$ refers to the state to be tracked, and the diagonal covariance matrix corresponding to the multi-frequency noise, $\mathbf{n}_k$, is defined as

$$\mathbf{R}_k = \text{diag}(\sigma_{n_{L1},k}^2, \sigma_{n_{L2},k}^2, \sigma_{n_{L5},k}^2). \quad (9)$$

or equivalently for the real form observation model,

$$\mathbf{R}_k = \text{diag}(\sigma_{n_{L1},k}^2, \sigma_{n_{L1},k}^2, \sigma_{n_{L2},k}^2, \sigma_{n_{L2},k}^2, \sigma_{n_{L5},k}^2, \sigma_{n_{L5},k}^2)/2. \quad (10)$$

Considering the strong scintillation scenario, analyzed in Section II-A. The scintillation complex gain components are approximated using an $\{$AR(3), AR(1)$\}$ model ($j = \{1, 2, 5\}$)

$$\begin{aligned} \rho_{s,k}^{L_j} &= \gamma_1^{L_j}\rho_{s,k-1}^{L_j} + \gamma_2^{L_j}\rho_{s,k-2} + \gamma_3^{L_j}\rho_{s,k-3} + \kappa^{L_j} + \eta_{\rho,k}^{L_j}, \\ \theta_{s,k}^{L_j} &= \beta_1^{L_j}\theta_{s,k-1} + \eta_{\theta,k}^{L_j}, \end{aligned} \quad (11)$$

with $[\gamma_1^{L_j}, \gamma_2^{L_j}, \gamma_3^{L_j}, \beta_1^{L_j}, \sigma_{\eta_{\rho L_j}}^2, \sigma_{\eta_{\theta L_j}}^2]$ the set of parameters that characterize the scintillation model for each frequency. Using this approximation, the filter tracks

$$\mathbf{x}_k \doteq [\mathbf{x}_{d,k}\ \mathbf{x}_{L1,k}\ \mathbf{x}_{L2,k}\ \mathbf{x}_{L5,k}]^\top, \quad (12)$$

$$\mathbf{x}_{d,k} \doteq \left[\theta_{d,k}^{L_1}\ \theta_{d,k}^{L_2}\ \theta_{d,k}^{L_5}\ f_{d,k}\ f_{r,k}\right], \quad (13)$$

$$\mathbf{x}_{L_j,k} \doteq \left[\rho_{s,k}^{L_j}\ \rho_{s,k-1}^{L_j}\ \rho_{s,k-2}^{L_j}\ \theta_{s,k}^{L_j}\right]. \quad (14)$$

The LOS dynamic carrier phase state evolution

$$\mathbf{x}_{d,k} = \underbrace{\begin{pmatrix} 1 & 0 & 0 & 2\pi T_s & \pi T_s^2 \\ 0 & 1 & 0 & 2\pi\delta_{L_2}T_s & \pi\delta_{L_2}T_s^2 \\ 0 & 0 & 1 & 2\pi\delta_{L_5}T_s & \pi\delta_{L_5}T_s^2 \\ 0 & 0 & 0 & 1 & T_s \\ 0 & 0 & 0 & 0 & 1 \end{pmatrix}}_{\mathbf{F}_d} \mathbf{x}_{d,k-1} + \mathbf{v}_{d,k}, \quad (15)$$

where $\delta_{L_2} = f_{L_2}/f_{L_1}$, $\delta_{L_5} = f_{L_5}/f_{L_1}$ and $\mathbf{v}_{d,k} \sim \mathcal{N}(0, \mathbf{Q}_{d,k})$ stands for possible uncertainties or mismatches on the dynamic model. The scintillation state evolution is

$$\mathbf{x}_{L_j,k} = \underbrace{\begin{pmatrix} \gamma_1^{L_j} & \gamma_2^{L_j} & \gamma_3^{L_j} & 0 \\ 1 & 0 & 0 & 0 \\ 0 & 1 & 0 & 0 \\ 0 & 0 & 0 & \beta_1^{L_j} \end{pmatrix}}_{\mathbf{F}_{L_j}} \mathbf{x}_{L_j,k-1} + \boldsymbol{\kappa}_{L_j} + \mathbf{v}_{L_j,k}, \quad (16)$$

with $\mathbf{v}_{L_j,k} \sim \mathcal{N}(0, \mathbf{Q}_{L_j,k})$, $\mathbf{Q}_{L_j,k} \doteq \text{diag}(\sigma_{\eta_{\rho L_j}}^2, 0, 0, \sigma_{\eta_{\theta L_j}}^2)$. Finally, the complete state evolution equations reads,

$$\mathbf{x}_k = \underbrace{\text{diag}(\mathbf{F}_d, \mathbf{F}_{L_1}, \mathbf{F}_{L_2}, \mathbf{F}_{L_5})}_{\mathbf{F}_k} \mathbf{x}_{k-1} + \boldsymbol{\kappa} + \mathbf{w}_k, \quad (17)$$

where the Gaussian process noise is defined as $\mathbf{w}_k = [\mathbf{v}_{d,k}; \mathbf{v}_{L_1,k}; \mathbf{v}_{L_2,k}; \mathbf{v}_{L_5,k}]$, with diagonal covariance matrix

$$\mathbf{Q}_k = \text{diag}(\mathbf{Q}_{d,k}, \mathbf{Q}_{L_1,k}, \mathbf{Q}_{L_2,k}, \mathbf{Q}_{L_5,k}). \quad (18)$$

III. Joint Carrier Tracking and Scintillation Mitigation Methodology

Traditional architectures relying on well-known PLLs are in general not able to provide continuous and reliable phase tracking under severe scintillation conditions [9]. Both advanced PLL-based solutions [10] and standard KF-based methods [9], [11], do no solve what we called the estimation vs mitigation trade-off [4]. That is, all standard techniques keep track of the incoming signal complete phase, then being difficult to distinguish the phase contribution due to dynamics from the scintillation phase disturbance, thus providing poor scintillation mitigation capabilities. To overcome this limitation, a new tracking approach was proposed in [4], [5], where the scintillation physical phenomena is mathematically modeled using convenient AR processes and embedded in the filter formulation. In this article, we extend these results to the multi-frequency case.

The new multi-frequency state-space model (SSM) formulation including both dynamics, scintillation amplitude fades and phase contributions at three different frequencies is given by equations (7) and (17), and is characterized by the set of parameters $\left\{\beta_1^{L_j}, \gamma_1^{L_j}, \gamma_2^{L_j}, \gamma_3^{L_j}, \kappa_{L_j}, \sigma_{\eta_{\theta L_j}}^2, \sigma_{\eta_{\rho L_j}}^2\right\}_j$ for $j = \{1, 2, 5\}$, and $\{\mathbf{Q}_{d,k}, \sigma_{n_{L1},k}^2, \sigma_{n_{L2},k}^2, \sigma_{n_{L5},k}^2\}$. For each frequency, the $\{$AR(3), AR(1)$\}$ scintillation model approximation parameters can be computed offline using CSM time-series, by fitting AR models to scintillation amplitude and phase traces. $\mathbf{Q}_{d,k}$ is *a priori* fixed by the user from the expected dynamics, and $\sigma_{n,k}^2$ can be sequentially adjusted from the C/N_0 estimator available at the receiver [10]. We propose to use an EKF, which directly operates with the received signal complex samples, thus avoiding discriminator's nonlinearities, loss of Gaussianity and saturation at low C/N_0. Instead of directly using (6), we consider a real valued implementation (i.e., observation dimension= 6).

The main idea behind the EKF consists of linearizing the possibly nonlinear system functions around the predicted and

ISBN 978-0-9928626-7-1 © EURASIP 2017

updated state estimates, and then applying the standard linear KF equations. In this case, only the measurement equation is nonlinear, which can be expressed in a real valued form as

$$\mathbf{h}_k(\mathbf{x}_k) = \begin{bmatrix} A_k^{L_1}\rho_{s,k}^{L_1}\cos(\theta_{d,k}^{L_1}+\theta_{s,k}^{L_1}) \\ A_k^{L_1}\rho_{s,k}^{L_1}\sin(\theta_{d,k}^{L_1}+\theta_{s,k}^{L_1}) \\ A_k^{L_2}\rho_{s,k}^{L_2}\cos(\theta_{d,k}^{L_2}+\theta_{s,k}^{L_2}) \\ A_k^{L_2}\rho_{s,k}^{L_2}\sin(\theta_{d,k}^{L_2}+\theta_{s,k}^{L_2}) \\ A_k^{L_5}\rho_{s,k}^{L_5}\cos(\theta_{d,k}^{L_5}+\theta_{s,k}^{L_5}) \\ A_k^{L_5}\rho_{s,k}^{L_5}\sin(\theta_{d,k}^{L_5}+\theta_{s,k}^{L_5}) \end{bmatrix}. \quad (19)$$

The linearized measurement matrix (6×17) to be used in the KF measurement update step is[2]

$$\tilde{\mathbf{H}}_k = \nabla \mathbf{h}_k(\hat{\mathbf{x}}_{k|k-1}) = \left[\tilde{\mathbf{H}}_{d,k}, \tilde{\mathbf{H}}_{L_1,k}, \tilde{\mathbf{H}}_{L_2,k}, \tilde{\mathbf{H}}_{L_5,k}\right],$$

with the different matrices given in equations (20)-(23). Note that the matrix is evaluated at the predicted state, $\mathbf{x}_k = \hat{\mathbf{x}}_{k|k-1}$, with $\hat{\theta}_{k|k-1}^{L_j} \doteq \hat{\theta}_{d,k|k-1}^{L_j} + \hat{\theta}_{s,k|k-1}^{L_j}$[3]. It is worth saying that it's straightforward to construct a double-frequency version of this SSM formulation, to consider the L_1/L_2, L_1/L_5 or L_2/L_5 pairs.

IV. Computer simulations

The performance of the new multi-frequency KF-based carrier tracking method (i.e., named MFEKF-AR in the simulations) is analyzed using synthetic strong scintillation CSM data. The results are compared to the current discrimantor-based state-of-the-art techniques, i) 3^{rd} order PLL with an equivalent bandwidth $B_w = 5$ Hz, ii) Standard KF, and iii) Adaptive KF (AKF), adjusting the measurement noise variance from the C/N_0 estimate; together with iv) the scalar AKF-AR presented in [4], only tracking the scintillation phase, and v) the scalar EKF-AR presented in [5], tracking both scintillation amplitude and phase. We consider a rapidly varying Doppler profile given by an initial random phase in $[-\pi, \pi]$, initial Doppler $f_{d,0} = 50$ Hz and constant rate $f_{r,0} = 100$ Hz/s. The signal is sampled at $T_s = 10$ ms and received with $C/N_0 = 30$ dB-Hz. The measure of performance is the root mean square error (RMSE) on the L1 carrier phase, $\theta_{d,k}^{L_1}$, averaged over 500 runs.

We consider three different strong scintillation scenarios, with the following parameters for the three GPS frequency bands: Case #1 with $S_4 = 0.7$ and $\tau_0 = 0.3$; Case #2 with $S_4 = 0.8$ and $\tau_0 = 0.2$; and Case #3 with $S_4 = 0.9$ and $\tau_0 = 0.1$. The steady-state (i.e., after convergence) RMSE obtained with the new MFEKF-AR is shown in Figure 2, where also the performance of the scalar version of the EKF [5] is given as a reference. In all the tested scenarios, taking into account multi-frequency observations implies a performance improvement, thus providing better scintillation mitigation capabilities. The mean RMSE results obtained with the rest of the methods considered in this study are summarized in Table I. Standard techniques are not able to correctly estimate the dynamics' phase of interest because they track the complete phase, including both phase contributions.

Regarding the methods including the AR scintillation approximation into the state-space model formulation, a huge performance gain is obtained when considering an EKF formulation. Also, taking into account not only the scintillation phase but its amplitude fadings in the filter formulation may prove very valuable for scintillation mitigation. It might be possible to use this high-rate estimation of amplitude to influence down-stream receiver functionality, in data recovery methods such as the SOVA decoder, or simply in terms of observation processing, including instantaneous weighting or rejection of carrier phase measurements. Overall, the new multi-frequency approach tracking both the dynamics' phase and ionospheric scintillation components is a promising solution for high-precision GNSS receivers.

Scintillation	Case #1	Case #2	Case #3
PLL	0.6330	0.8315	1.1195
KF	0.4899	0.5952	0.7856
AKF	0.4578	0.5222	0.5970
AKF-AR	0.4617	0.4323	0.4022
EKF-AR	0.0843	0.0935	0.0967
MFEKF-AR	0.0648	0.0694	0.0728

TABLE I
STEADY-STATE RMSE (RAD) PERFORMANCE OBTAINED WITH 6 DIFFERENT TECHNIQUES FOR 3 SEVERE SCINTILLATION SCENARIOS.

V. Conclusions

This article presented a new state-space formulation for the multi-frequency carrier phase tracking problem. The final goal was to obtain a robust framework and tracking methodology for strong ionospheric scintillation mitigation. To overcome the limitations of standard techniques, both scintillation components were modeled using AR processes and embedded into the state-space formulation. This allowed the filter to track independently the dynamic phase of interest and the scintillation phase disturbances, providing effective scintillation mitigation capabilities. The performance of the new approach was compared to standard PLL and KF-based scalar tracking techniques in challenging propagation scenarios, and was shown to outperform these techniques and thus being a promising approach for high-precision receivers.

Acknowledgment

This work has been supported by the Spanish Ministry of Economy and Competitiveness through project TEC2015-69868-C2-2-R (ADVENTURE) and by the Government of Catalonia under Grant 2014–SGR–1567.

References

[1] M. G. Amin, P. Closas, A. Broumandan, and J. L. Volakis, "Vulnerabilities, threats, and authentication in satellite-based navigation systems [scanning the issue]," *Proceedings of the IEEE*, vol. 104, no. 6, pp. 1169–1173, June 2016.

[2] The vector differential operator is defined as $\nabla = \left[\frac{\partial}{\partial x_1}, \ldots, \frac{\partial}{\partial x_N}\right]$.

[3] $_{k|k-1}$ refers to the predicted estimate at time k using measurements up to time $k-1$, and $_{k|k}$ refers to the estimated value at time k using measurements up to time k.

$$\tilde{\mathbf{H}}_{d,k} = \begin{bmatrix} -A_k\hat{\rho}^{L_1}_{s,k|k-1}\sin(\hat{\theta}^{L_1}_{k|k-1}) & 0 & 0 & 0 & 0 \\ A_k\hat{\rho}^{L_1}_{s,k|k-1}\cos(\hat{\theta}^{L_1}_{k|k-1}) & 0 & 0 & 0 & 0 \\ 0 & -A_k\hat{\rho}^{L_2}_{s,k|k-1}\sin(\hat{\theta}^{L_2}_{k|k-1}) & 0 & 0 & 0 \\ 0 & A_k\hat{\rho}^{L_2}_{s,k|k-1}\cos(\hat{\theta}^{L_2}_{k|k-1}) & 0 & 0 & 0 \\ 0 & 0 & -A_k\hat{\rho}^{L_5}_{s,k|k-1}\sin(\hat{\theta}^{L_5}_{k|k-1}) & 0 & 0 \\ 0 & 0 & A_k\hat{\rho}^{L_5}_{s,k|k-1}\cos(\hat{\theta}^{L_5}_{k|k-1}) & 0 & 0 \end{bmatrix} \tag{20}$$

$$\tilde{\mathbf{H}}_{L1,k} = \begin{bmatrix} A_k\cos(\hat{\theta}^{L_1}_{k|k-1}) & 0 & 0 & -A_k\hat{\rho}^{L_1}_{s,k|k-1}\sin(\hat{\theta}^{L_1}_{k|k-1}) \\ A_k\sin(\hat{\theta}^{L_1}_{k|k-1}) & 0 & 0 & A_k\hat{\rho}^{L_1}_{s,k|k-1}\cos(\hat{\theta}^{L_1}_{k|k-1}) \\ \mathbf{0}_{4x1} & \mathbf{0}_{4x1} & \mathbf{0}_{4x1} & \mathbf{0}_{4x1} \end{bmatrix} \tag{21}$$

$$\tilde{\mathbf{H}}_{L2,k} = \begin{bmatrix} \mathbf{0}_{2x1} & \mathbf{0}_{2x1} & \mathbf{0}_{2x1} & \mathbf{0}_{2x1} \\ A_k\cos(\hat{\theta}^{L_2}_{k|k-1}) & 0 & 0 & -A_k\hat{\rho}^{L_2}_{s,k|k-1}\sin(\hat{\theta}^{L_2}_{k|k-1}) \\ A_k\sin(\hat{\theta}^{L_2}_{k|k-1}) & 0 & 0 & A_k\hat{\rho}^{L_2}_{s,k|k-1}\cos(\hat{\theta}^{L_2}_{k|k-1}) \\ \mathbf{0}_{2x1} & \mathbf{0}_{2x1} & \mathbf{0}_{2x1} & \mathbf{0}_{2x1} \end{bmatrix} \tag{22}$$

$$\tilde{\mathbf{H}}_{L5,k} = \begin{bmatrix} \mathbf{0}_{4x1} & \mathbf{0}_{4x1} & \mathbf{0}_{4x1} & \mathbf{0}_{4x1} \\ A_k\cos(\hat{\theta}^{L_5}_{k|k-1}) & 0 & 0 & -A_k\hat{\rho}^{L_5}_{s,k|k-1}\sin(\hat{\theta}^{L_5}_{k|k-1}) \\ A_k\sin(\hat{\theta}^{L_5}_{k|k-1}) & 0 & 0 & A_k\hat{\rho}^{L_5}_{s,k|k-1}\cos(\hat{\theta}^{L_5}_{k|k-1}) \end{bmatrix} \tag{23}$$

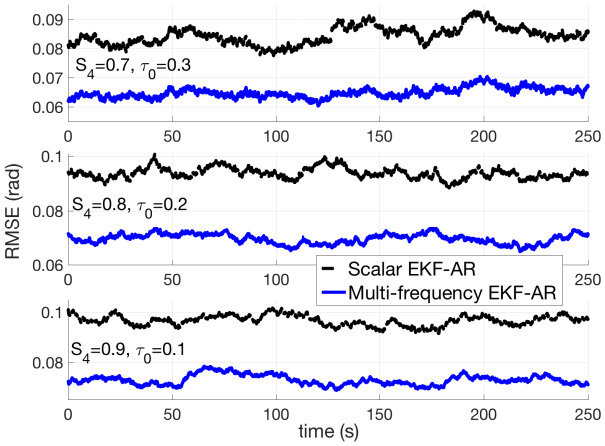

Fig. 2. Steady-state RMSE (rad) performance obtained with the new MFEKF-AR and the scalar EKF-AR for the 3 strong scintillation scenarios.

[2] P. M. Kintner et al., "GNSS and ionospheric scintillation. How to survive the next solar maximum," *Inside GNSS*, pp. 22–33, July/Aug. 2009.

[3] T. E. Humphreys et al., "Simulating ionosphere-induced scintillation for testing GPS receiver phase tracking loops," *IEEE Journal of Selected Topics in Signal Processing*, vol. 3, no. 4, pp. 707–715, Aug. 2009.

[4] J. Vilà-Valls, P. Closas, C. Fernández-Prades, J. A. López-Salcedo, and G. Seco-Granados, "Adaptive GNSS carrier tracking under ionospheric scintillation: estimation vs mitigation," *IEEE Communications Letters*, vol. 19, no. 6, pp. 961–964, June 2015.

[5] J. Vilà-Valls, P. Closas, and C. Fernández-Prades, "Advanced KF-based methods for GNSS carrier tracking and ionospheric scintillation mitigation," in *Proc. of the IEEE Aerospace Conference*, Big Sky, MN, March 2015, DOI: 10.1109/AERO.2015.7118930.

[6] M. Petovello, "Would you prefer to have more satellites or more signals?," *Inside GNSS*, pp. 45–47, Mar/Apr 2017.

[7] S. M. Kay, *Fundamentals of Statistical Signal Processing: Estimation Theory*, Prentice-Hall, Englewood Cliffs, New Jersey, USA, 1993.

[8] S. Locubiche-Serra, G. Seco-Granados, and J. A. López-Salcedo, "Doubly-adaptive autoregressive Kalman filter for GNSS carrier tracking under scintillation conditions," in *Proc. of the ICL-GNSS*, 2016.

[9] T. E. Humphreys et al., "GPS carrier tracking loop performance in the presence of ionospheric scintillations," in *Proc. of the ION GNSS*, Long Beach, CA, Sept. 2005, pp. 156–167.

[10] J. López-Salcedo, J. Peral-Rosado, and G. Seco-Granados, "Survey on robust carrier tracking techniques," *IEEE Commun. Surveys & Tutorials*, vol. 16, no. 2, pp. 670–688, April 2014.

[11] C. Macabiau et al., "Kalman filter based robust GNSS signal tracking algorithm in presence of ionospheric scintillations," in *Proc. of ION GNSS*, Nashville, TN, Sept. 2012, pp. 3420 – 3434.

ISBN 978-0-9928626-7-1 © EURASIP 2017